EUCLIPSE

EU Cloud Intercomparison, Process Study & Evaluation Project

Grant agreement no. 244067

Deliverable D3.6:	Results at selected grid points (GCPI/CloudNet/ARM/AMMA)
Delivery date:	18 months
Responsible partner:	KNMI

D3.6 Compilation of ESM results at selected grid points (De Roode, Neggers, Guichard and Siebesma)

1. Introduction

One of the main aims of WP3 is to evaluate how the large-scale forcing conditions control cloud cover, cloud amount, precipitation, and how these cloud properties influence the radiative budget. In this report we summarize the results of studies that focus on the model representation of clouds in a subset of the GEWEX Pacific Cross Section Intercomparison (GPCI, Dal Gesso et al., 2014b), AMMA and the CloudNet site of Cabauw (Neggers and Siebesma, 2013).

Clouds are often generated by processes that act on spatial and temporal scales that are much smaller than the scales of discretization in Earth System Models (ESMs), and as a consequence their impact has to be represented through parameterization. Great variety exists among the suites of subgrid parameterizations in the various present-day operational ESMs. On the one hand, this reflects the long history of the scientific research behind their formulation, going back decades. On the other hand, this variety reflects the significant complexity of such parameterization schemes, which typically consist of many individual parametric functions, each representing an observed statistical relation between one quantity and another. This complexity brings some considerable risks. The first is in transparency, that is, the interaction between the many parametric components is often not fully understood, which might result in unexpected behavior or instability in the model. Another risk is that of introducing so-called compensating errors between parametric components. These are situations in which a structural error by one component is erroneously compensated by another.

In a shifting future climate, when each process might act differently, it is not guaranteed that such an artificial correction will still hold. Another potential side effect of compensating errors is that the improvement of one parametric component does not guarantee an improvement in the overall ESM performance. Neggers and Siebesma (2013) used a wide variety of Cabauw observations aiming to improve the detection of compensating errors in parameterization schemes with an emphasis on the representation of clouds. In particular, they investigate how differences in biases between models for multiple variables reflect how a change in the representation of one parameter (say, cloud cover) impacts another through a chain of interacting fast processes (such as the surface turbulent fluxes of heat and moisture).

A second study investigates the representation of low clouds in a selected part of the GPCI area. In particular it is questioned how the free tropospheric temperature and specific humidity control the low cloud amount in SCM versions of ESMs. This is motivated by an analysis of the conditions above the inversion layer from ERA-Interim carried out by Dal Gesso et al. (2014) and results from the Lagrangian model intercomparison cases. The Lagrangian transition model intercomparison study, reported in detail in the Deliverables 3.3 and 3.4, showed that LES models agreed very well on the timing of the break-up of the stratocumulus clouds. By contrast, there is a strong disagreement between the SCM results. From an inspection of the cloud fraction on the inversion jumps of heat ($\Delta\theta_l$) and moisture (Δq_t) through a single stability parameter κ,

$$\kappa \equiv 1 + \frac{c_p}{L_v}\frac{\Delta\theta_l}{\Delta q_t} \qquad (1)$$

it was found that the results for the intercomparison cases agree remarkable well with those obtained for the GEWEX Pacific Cross Section Intercomparison Project (GPCI) from a free climate run (see Figure 1.1). This has motivated a study that extends the CGILS experiments by investigating in detail the dependency of the cloud amount on a wide range of values for the inversion jumps of both humidity and heat.

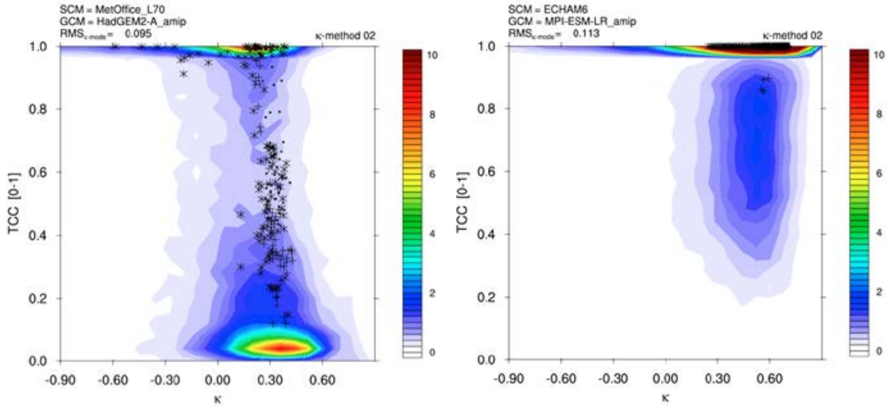

Fig. 1.1: The cloud cover as a function of the inversion stability factor κ defined by Eq. (1). The crosses were obtained from SCM runs of the four GASS-EUCLIPSE Lagrangian cloud transition cases, whereas the results shown in colors indicate results from CMIP5 (left HadGEM2 and right MPI).

Last, AMMA

The set-up of the report is as follows. Sections 2, 3, and 4 summarizes the findings of Neggers and Siebesma (2013), Dal Gesso et al. (2014b) and a follow up of the study by Roehrig et al. (2013), respectively. We present our concluding remarks in Section 5.

2. Using CloudNet data to trace compensating errors between cloud vertical structure and cloud overlap

Neggers and Siebesma (2013) propose a new strategy that consists of the continuous, long-term simulation and evaluation of single-column models (SCMs) against a multitude of independently measured parameters at meteorological supersites (see Table 2.1). In particular, they aim to improve the detection of compensating errors in parameterizations. In their paper they explain how errors in cloud amount and cloud cover can compensate such to give reasonable values for the downwelling SW.

	Parameter	Abbreviation	Units	Instrument
1	Total cloud cover	TCC	%	CloudNet
2	Downward shortwave radiative flux at sfc	SW_d	$W\,m^{-2}$	BSRN
3	Downward longwave radiative flux at sfc	LW_d	$W\,m^{-2}$	BSRN
4	Sensible heat flux at 5 m	SHF	$W\,m^{-2}$	Sonic anemometer and thermometer
5	Latent heat flux at 5 m	LHF	$W\,m^{-2}$	Sonic anemometer and optical open-path sensor
6	Soil temperature at 0 cm	T_{soil}	K	KNMI nickel-wired needles
7	Air temperature at 2 m	T_{2m}	K	KNMI Pt500
8	Air temperature at 200 m	T_{200m}	K	KNMI Pt500
9	Lowest cloud-base height	z_{base}	m	LD40 ceilometer and LES
10	Maximum cloud fraction within BL	cf_{max}	%	LES
11	Height of maximum cloud fraction	z_{cfmax}	m	LES
12	Cloud overlap ratio	$r_{overlap}$	—	LES

Table 2.1. Set of observed and LES-diagnosed parameters at Cabauw used in the SCM evaluation. sfc: surface; BSRN: Baseline Surface Radiation Network.

The set of parameters used in this study for model evaluation is chosen to reflect the cloud, radiative, and thermodynamic state of the atmospheric boundary layer, as well as the surface heat budget and the soil temperature. The 12 data streams as listed in Table 1 consist of two types, namely, (i) measurements by instrumentation at Cabauw and (ii) LES results at Cabauw. The observational parameters are routinely measured at Cabauw and are therefore available for long and continuous periods of time. The LES data supplement this set with information on key aspects of cloud structure for which no measurements are available.

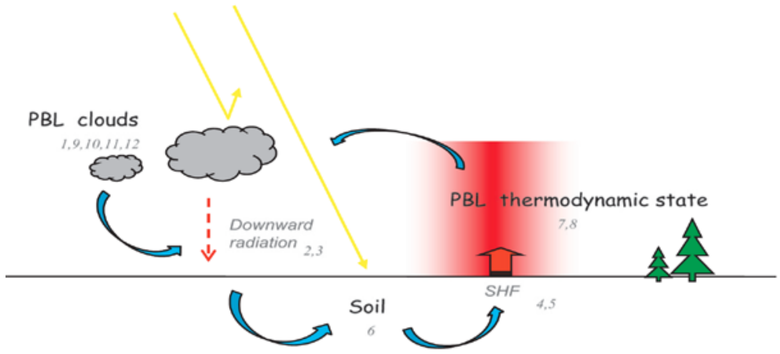

Figure 2.1. Schematic illustration of the chain of interacting processes in the coupled soil–BL system that is investigated. Numbers refer to the 12 measurements and LES diagnostics as listed in Table 1 that are used to constrain this system.

The chosen set of 12 parameters is designed to constrain the following impact mechanism in the coupled boundary layer–soil system, which mainly involves fast physics and thus acts on very short time scales. This mechanism is schematically illustrated in Fig. 2.1. It is suspected from preliminary tests for various idealized cases that the representation of boundary layer clouds by the new scheme will differ considerably from the control model, both in amount and in vertical structure. Suppose such a difference will also materialize in multi-year simulations with the SCM at Cabauw. This difference in clouds will affect the radiative transfer through the atmosphere, which should affect the surface downward radiative fluxes. These are part of the surface energy budget, which will affect both the surface temperature and the surface sensible heat flux. Last, this will impact the low-level temperature in the atmospheric boundary layer. All main processes in this chain of fast interactions thus react to a change in cloud representation; at the same time, the state of these processes is also routinely measured at Cabauw or can be estimated from LES simulations. This allows constraining the representation of this interactive chain at multiple points (as indicated in Fig. 2.1), and thus identifying possible compensating errors between them.

One could argue that many more parameterizations are involved in this chain of interactions than there are measurements. Accordingly, some compensating errors might still remain undetected. However, using 12 independent measurements is already an improvement from evaluating against a single measurement, such as, say, total cloud cover—many examples of the latter type of model evaluation already exist in the literature. The first improvement is that confronting a model with multiple independent measurements should give the investigator more confidence in the result compared to a single-variable evaluation. Second, evaluations for a limited number of parameters can already be successful at revealing compensating errors at the first-order level, that is, between the main components in the interacting system. More generally speaking, this analysis procedure should be interpreted as a first attempt at constraining a system of interacting parameterizations more comprehensively—somewhat limited (but not complicated) by the measurements that are currently available.

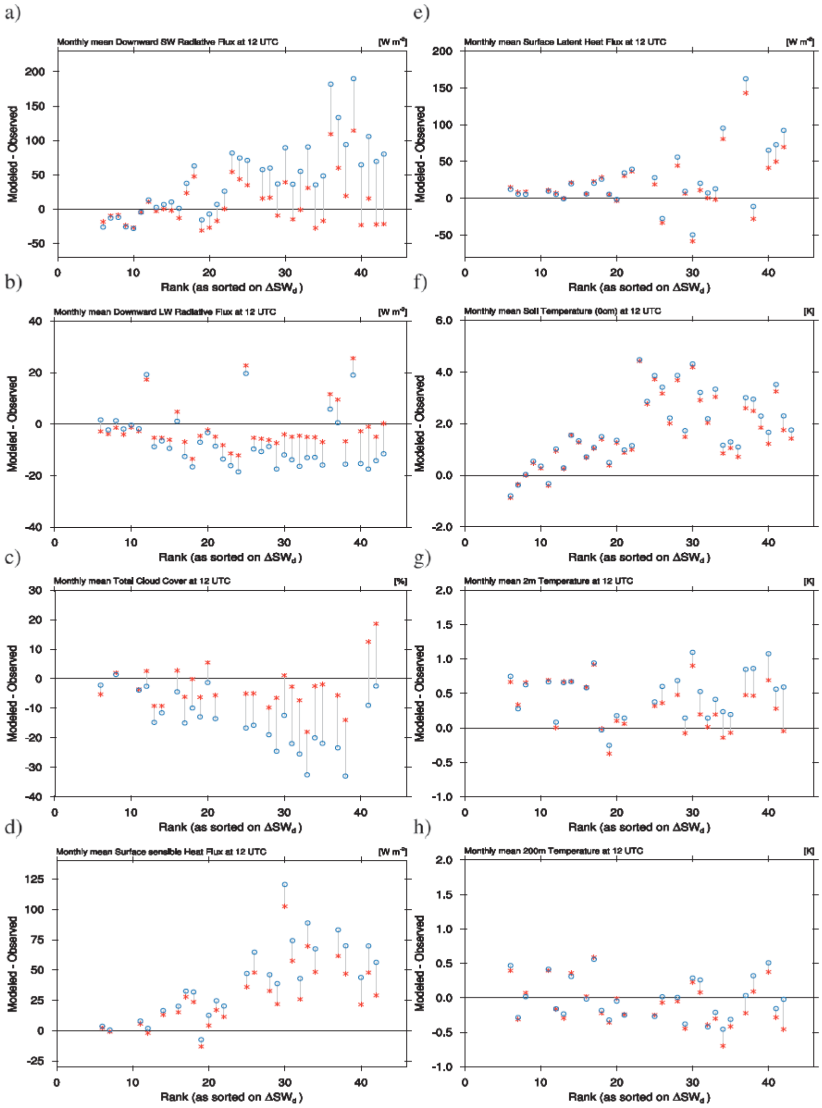

Figure 3. Modeled-observed monthly-mean values of (a)–(h) the eight chosen variables plotted as a function of the rank in the difference in SW_d between the new (blue) and control (red) SCM for the period 2007–10. Gray line connecting the red and blue symbols indicates the change in the bias as a result of the implementation of the new BL scheme.

The nature of this impact mechanism is investigated in more detail in Fig. 3, which shows results obtained from two parameterizations schemes. One is identical to that of the ECMWF model cycle 31R1, whereas the other includes an eddy diffusivity mass flux (EDMF) approach (Neggers et al., 2009; Neggers 2009). The two SCM versions are run for the period covering 2007-2010. The figure adopts a special plotting method. On the vertical axis the modeled-minus-observed value is shown. This highlights the difference between models, but it simultaneously maintains information about the measurement. In addition, on the horizontal axis the monthly means are now sorted on the associated difference in the downwelling shortwave radiation (SW_d) between the two models. As a result, each data point (representing the mean over a specific month) has the same position on the horizontal axis in all panels. What this reveals is that the difference in bias between the two models increases with rank for all parameters in this set— with the largest differences on the right-hand side. This suggests that the impacts on all parameters are related to the change in SW_d, and that clear correlations should exist between model differences in various variables.

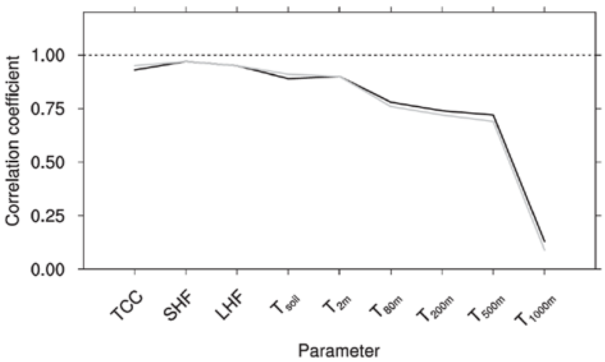

Figure 4. Correlation coefficients between the monthly-mean model differences in SW_d and various other variables for the period 2007–2010. Black line represents Pearson's correlation coefficient, while gray line represents Spearman's rank correlation coefficient.

Figure 4 lists the correlation coefficients between the model difference in SW_d and all other variables. Comparing the degree of correlation among variables provides further insight into where this impact mechanism starts, and how deeply it works its way into the coupled boundary layer–soil system. For example, the model difference in the surface downward shortwave radiation is highly correlated to the model differences in cloud cover. The correlations between SW_d and the surface heat fluxes are similarly high, reflecting a substantial impact on the surface energy budget. However, the correlation between SW_d and the soil temperature, as well as the air temperature at 2m, is already somewhat weaker; and then it further weakens with height above the surface. At 1-km height the correlation coefficient has reduced to only 0.13. In general, the correlation weakens when a process is further down the chain of interacting processes, reflecting that other processes also start to play a role; in the case of air temperature, this probably reflects a difference in the vertical structure of the thermodynamic state, directly resulting from the use of a different model for boundary layer transport and cloud. It is noted that both models use the same microphysics and cloud overlap schemes—only the representation of the macrophysical cloud structure was changed. So, the results presented so far do strongly suggest that the change in cloud fraction drives the changes in radiation and other parameters.

As a next step observed shallow cumulus cases will be compared to the SCM results. To this purpose an additional set of four relevant variables is defined that reflects the key aspects of the cloud vertical structure in which the two SCM versions differ: the cloud–base height, the maximum cloud fraction in the boundary layer, the height of maximum cloud fraction in the boundary layer, and the boundary layer cloud overlap ratio. The latter is defined as the maximum cloud fraction over total cloud cover, both diagnosed over the lowest 4 km. The overlap ratio is included in this set because of its potentially important impact on radiative transfer.

The EDMF model performs significantly better for the cloud-base height, the maximum cloud fraction, and the height of the maximum cloud fraction. The maximum cloud fraction, in particular, seems to be overpredicted by the control model; it is unable to reproduce the small amplitudes typical of fair-weather cumulus as diagnosed in the LES. Interestingly, both models perform poorly for the cloud overlap ratio, as expressed by the shared large bias for this parameter. On average, the SCMs give $r_{overlap} = 1$, while the LES gives $r_{overlap} = 0.5$; in other words, the SCMs in effect apply the maximum overlap limit (i.e., total cover equals maximum fraction), while in the LES the overlap is much less efficient.

2.1 Discussion of the results

The better performance by the new model on boundary layer cloud structure, in combination with the worse performance for all other variables, might seem paradoxical at first. However, this apparent contradiction is explained by the shared error on cloud overlap. Similar to most operational GCMs, the maximum-random overlap function is applied in the radiation scheme in RACMO. This overlap function was not affected by the implementation of the new boundary layer scheme, so that both model versions use the same overlap function. In the case of the ECMWF C31R1 parameterization scheme, the overestimation of the maximum cloud fraction in the boundary layer is compensated by the assumption of too efficient vertical overlap, resulting in a still reasonable estimate of the projected cloud cover (but for the wrong reason). In contrast, the new EDMF scheme better reproduces the smaller cloud fractions, as seen in the LES; but in the radiation scheme, this is still combined with the too efficient.

Other topics can be studied using the method followed in this study, although some terms and conditions apply. The process of interest should act on time and length scales small enough so that (i) the phenomenon acts much faster than the atmospheric circulation in which it is embedded and (ii) it is 'locally forced' enough to allow its study in the absence of interaction with the larger scales. Only then can the problem be addressed with single-column modeling using prescribed large-scale forcings. Examples of topics that could be studied are (i) the representation of momentum transport in the boundary layer, (ii) the humidity budget of the boundary layer (left out of this study for the sake of simplicity and unity of topic), and (iii) impacts of soil moisture on evaporation. An example of a process that is less appropriate to study is mature deep convection, as this often involves mesoscale effects that might be partially resolved in the associated GCM.

In practice, another limiting factor in multiple-parameter evaluation at process level often proves to be the availability of instrumentation at a site, or the insufficient time coverage of the relevant measurements. The approach described here advocates the long-term, continuous measurement of a range of relevant variables at supersites, and promotes their availability to the scientific community. In this study LES-generated datasets were used to supplement the observational datasets on parameters required to solve the problem. However, one should realize that LES is still a model. It should itself be evaluated against measurements, to increase confidence in its use as a virtual laboratory. The evaluation of a system of interacting fast-acting parameterizations in isolated mode from the larger-scale circulation against long-term measurements at permanent meteorological sites can facilitate the attribution of GCM behavior to specific parameterizations.

3. GEWEX Pacific Cross Section

The representation of the stratocumulus cloud amount in SCMs for a wide range of free tropospheric conditions that are representive for the GEWEX Pacific Cross Section Intercomparison Project (GPCI) and a comparison to LES results is reported in detail by Dal Gesso et al. (2014b). This work is partly motivated by Fig. 5, which shows a joint PDF of lower tropospheric stability (LTS) and the bulk humidity difference between the 700 hPa level and the surface (ΔQ) for the stratocumulus area of the NE-Pacific. Six SCMs are evaluated on the basis of their representation of the dependence of the stratocumulus-topped boundary layer regime on the free tropospheric thermodynamic conditions and a comparison is made to results obtained with the Dutch Atmospheric LES model (DALES). The GCM counterparts of five SCMs participated to the Coupled Model Intercomparison Project version 5 (CMIP5), while HadGEM3 is the latest release of the climate model developed at the Met Office and will participate to CMIP6.

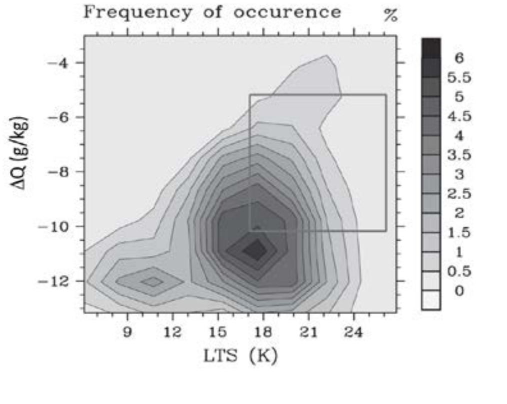

Figure 5. Joint PDF of night-time data from ERA-Interim for the summertime (June, July, August) between 1979 and 2012. The data are sampled in the California area of stratocumulus (20–30^{0}N, 120–130^{0}W) and for the meteorological conditions corresponding to the subsidence regime and SST within 0.5K of the considered values in Table 1. The box indicates the area of the phase space considered in the present study.

Set up of the experiments

Table 1 shows the mean forcing conditions. For simplicity no mean horizontal advection of heat and moisture is applied. The LES and SCM runs last 10 and 100 days, respectively.

Position	32°N, 129°W
Date	15 July 2003
Incoming short-wave radiation ($W m^2$)	471.5
Zenith angle (°)	52
Surface albedo	0.07
p_s (hPa)	1012.8
SST (K)†	292/294
$q_{t,0}$ ($g kg^{-1}$)†	13.4/15.1
U_G ($m s^{-1}$)	0
V_G ($m s^{-1}$)	−6.74
w_0 ($mm s^{-1}$)	3.5
z_w (m)	500
σ_w (−)	0.5

Table 1. Set-up of the experiments for the control case. In the perturbed cases the SST increased by 2K.

Control simulations

The mean states of the CC and LWP (Fig. 6) are examined for the experiment with an additional stochastic noise added to the subsidence. In particular, following Bellon and Stevens (2012) the variation of the subsidence with height is given by

$$W_{subs} = -w_0(1+w(t))[1-\exp(-z/z_w)] \quad , \quad (2)$$

which acts to balance the radiative cooling in the free troposphere. The quantity w(t) is a random number which varies between σ_w and $-\sigma_w$.

For some cases corresponding to humid and cool free tropospheric conditions (upper-left corner of the phase space) a cloud layer forms above 3 km because of the generation of energetic plumes. HadGEM2, HadGEM3, LMDZ-AR4 and CNRM-CM5 present this feature. As the presence of a high-level cloud layer above the Scu-topped boundary layer is beyond the interest of this paper, those cases are excluded from our analysis. The patterns of CC (Fig. 6) in the phase space differ noticeably from model to model. However the model fingerprint is rather distinct and is not strongly affected by the additional stochastic noise added to the subsidence. EC-EARTH, HadGEM2, and CNRM-CM5 present a fairly constant CC=1 in a large area of the phase space. A CC reduction is found in the lower-left corner of the phase space. LMDZ-AR4 exhibits a constant CC in the phase space. MIROC5 shows a net increase in the CC towards weaker LTS and moister free tropospheric conditions. A similar behaviour is found for HadGEM3 even though for different reasons. In fact HadGEM3 presents a wide region of the phase space corresponding to stronger LTSs with CC lower than 10%. For these cases the cloud layer slowly dissolves and once the boundary layer becomes clear it warms quickly and becomes stably stratified. In the absence of the horizontal advection of cold and dry air, the cloud layer cannot reform again. Sensitivity studies (not shown) clarified that the cloud scheme is the main responsible for this extreme behaviour. When replaced by the scheme used in the older version of the model such a massive cloud loss is not found.

The spread in the LWP among the models is even more distinct than for the CC patterns. Also for this quantity the model fingerprint is not strongly affected by the stochastic noise added to the subsidence. None of the SCMs completely capture the LWP dependence on the free tropospheric conditions found in LES results performed by van der Dussen et al. (2014). More precisely they collectively fail to exhibit a decrease of LWP with increasing ΔQ. EC-EARTH and HadGEM2 exhibit a LWP increase for a weaker LTS and a drier free troposphere in the region of the phase space corresponding to a totally overcast boundary layer. The abrupt decrease in LWP in the lower-left corner of the phase space corresponds to a CC reduction. HadGEM3 shows a net increase in LWP towards weaker LTSs due to the wide region corresponding to the clear sky regime. A rather constant pattern is shown by LMDZ-AR4. For CNRM-CM5 the only noticeable variation is due to the cloud break-up in the lower-left corner of the phase space due to the selected colour scale. In the region corresponding to a totally overcast boundary layer, the LWP depends mainly on LTS and increases for a weaker LTS. Similarly to CNRM-CM5, MIROC5 presents a LWP pattern which is almost independent of ΔQ and increases for a weaker LTS. It is worth mentioning that in Dal Gesso et al. (2014a) larger differences between the results obtained with a constant subsidence in time and one including an additional stochastic noise were found. The study was conducted with the SCM version of EC-EARTH but with a higher resolution grid. The results suggest that the considered noise is probably too weak to strongly affect the patterns for course vertical resolutions such as the considered ones.

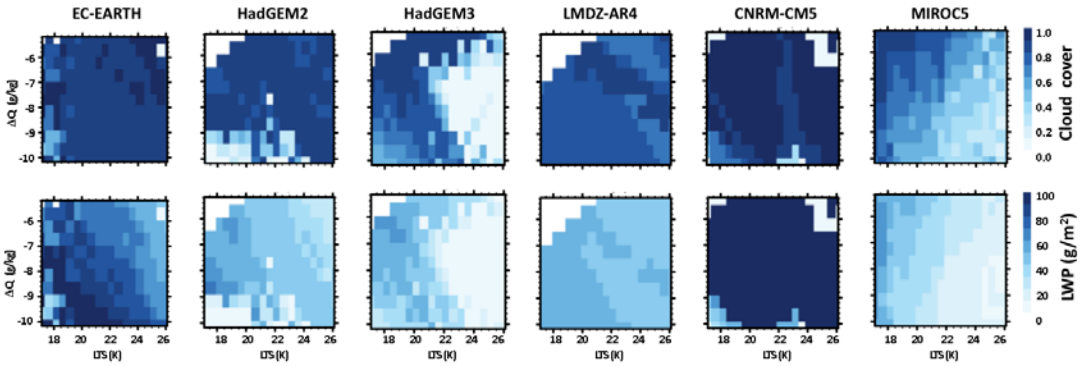

Figure 6. Cloud cover (CC) and LWP as obtained from six different SCMs. The results were obtained using a time-varying subsidence and represent mean values during the last 80 days of the simulations.

Stratocumulus response to a global warming scenario

To assess the effect of a perturbation in the large scale forcing on the SCM equilibria, the SST is increased by 2 K. A uniform warming of the free troposphere is imposed as in Rieck et al. (2012) so that the LTS does not change. Furthermore the initial relative humidity (RH) in the free troposphere is kept constant to the control case.

The cloud radiative effect (CRE) is defined as the difference between the net downward radiative flux at the top of the atmosphere in total sky and in clear sky conditions. In DALES the change in the CRE normalized by the change in the SST (dCRE/dSST) is positive in the whole phase space (Van der Dussen et al. 2014). Since no stratocumulus break-up is found, the cloud response is due to a reduced LWP. In the perturbed climate the boundary layer is deeper and has a smaller relative humidity causing a higher cloud base. The change in the cloud base height is found to be larger than the increase in the cloud top height. The strongest response is found for larger LTS values, for which the boundary layer is shallower and more well-mixed.

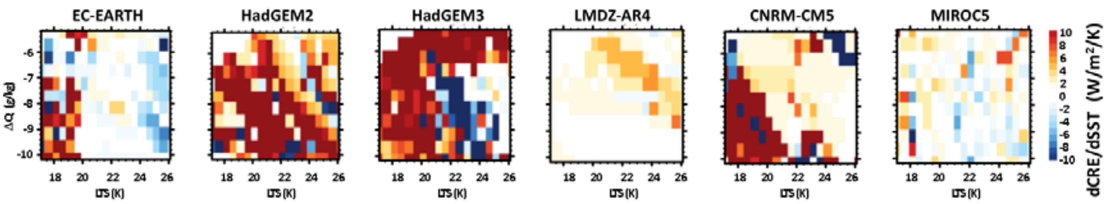

Figure 7. Mean cloud radiative feedback as a function of the LTS and ΔQ as obtained from the last 80 days of the SCM runs.

For small changes in the free tropospheric conditions, large changes in both the sign and the magnitude of the CRE response can be found (see Fig. 7). This results in a rather noisy pattern that does not show any clear dependence on LTS and ΔQ. The cloud feedback found with SCMs is due to changes in both the CC and the LWP. EC-EARTH, LMDZ-AR4 and MIROC5 do not present strong variations in the CC. More precisely EC-EARTH shows a CC decrease in the lower-left corner of the phase space only for the stochastic forcing experiment. A similar response is found for CNRM-CM5 for both the constant and stochastic forcing experiment. Moreover in the upper-right corner of the phase space a band with a net CC increase is found. These cases correspond to a clear-sky regime in the control climate experiment but show a totally overcast boundary layer in the perturbed climate experiment. In the regions of the phase space where the CC does not change the CRE response only depends on the change in the LWP. EC-EARTH presents a net LWP increase, while both LMDZ-AR4 and CNRM-CM5 predict a LWP decrease consistent with the LES results. For MIROC5, a rather scattered pattern is found for both CC and LWP. HadGEM2 exhibits a strong CC decrease in a large area of the phase space corresponding to drier free tropospheric conditions. For HadGEM3 a strong CC decrease is found for moister and warmer free tropospheric conditions (upper-right corner of the phase space). At the edge of the region corresponding to clear sky conditions in the control climate experiment, a band of stratocumulus-topped boundary layer cases is found with a consequent strong CRE decrease. Only two of the considered models participated to the CGILS model intercomparison study (Zhang et al., 2013), namely HadGEM2 and LMDZ-AR4.

3.1 Discussion

The present study applies an experimental design which is a simplified version of the CGILS set-up. In the CGILS project, horizontal advection of humidity and temperature are considered. Other details, such as the wind velocity and the subsidence, are more realistic than in the present study as based directly on observations. Furthermore in CGILS the climate perturbation includes a subsidence reduction, aimed to mimic the weakening of the Hadley circulation, which is neglected in the present study. However in Zhang et al. (2013) the predicted cloud feedback for experiment S12 (well-mixed stratocumulus) and S11 (decoupled stratocumulus) by HadGEM2 and LMDZ-AR4 is positive and a stronger response is given by HadGEM2. Therefore the general CRE response found in this study is in agreement with the CGILS results for HadGEM2 and LMDZ-AR4.

4. AMMA

A **west-Africa** transect (http://amma-mip.lmd.jussieu.fr) coinciding with the IOP of the AMMA campaign (Redelsperger et al. 2006) during which a wealth of surface and atmospheric observations are available allows critical evaluation of ESM simulations with the African Monsoon over this area.

Here in particular the climate model outputs, referred to as cfSites have been used extensively. These high-frequency model outputs, which incorporate thermodynamic budgets and fluxes, allow to conduct process-based evaluation of climate simulations. For West Africa, the locations of the cfSites have been defined so as to sample the meridional climatic gradient, from the Gulf of Guinea to the Sahara, plus the Western coastal Sahel (Figure 4.1). Many of these cfSites are close to observational sites where surface fluxes and/or soundings data have been collected. We have mainly focused on 30-year long AMIP runs to evaluate land and atmosphere physical processes in climate models. In the following, we illustrate our utilization of these outputs on an analysis of the surface-boundary layer-clouds couplings arising in models and observations. Note that some CNRM-CM5 and EC-Earth outputs are provided with a 3h-time sampling (instead of 30 min).

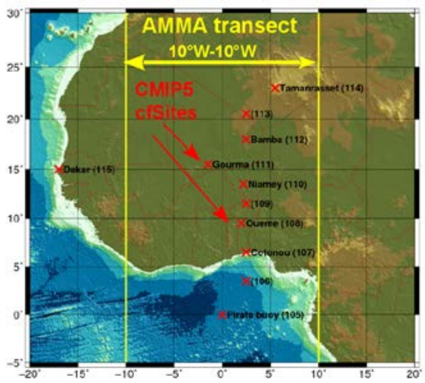

Figure 4.1. *Map showing the location of the CMIP5 CFMIP cfSites over West Africa (red crosses, with cfSites number in black).*

4.1 Diurnal cycle and thermodynamic couplings

Over land, the surface energy budget, boundary layers (BL) and clouds display large geographic, differences, with distinct annual and diurnal cycles (Guichard et al. 2009, Bouniol et al. 2012). In West Africa, during the monsoon, the atmospheric balance of the lower troposphere appears to be strongly shaped at large scale by deep convective processes within the ITCZ (intertropical convergence zone), by nocturnal advection associated with the monsoon flow on the northern warmer side of the ITCZ and by the cloud cover prevailing on the southern cooler side.

These various balances are coupled with distinct low-level thermodynamics and diurnal cycles of boundary layers which are well framed by consideration of the surface temperature and thermodynamic diagrams (Gounou et al. 2012, Couvreux et al. 2014). Away from the coast, as the surface becomes warmer, the specific humidity in the low levels, which is bounded by saturation, increases at first, but north of the ITCZ, where the boundary layer can display a strong daytime drying, the specific humidity overall decreases (Fig. 4.2, lower right panel).

Couvreux et al. (2014) showed with a one-dimensional model that the bias in simulated temperature and water vapor consistently change signs across these contrasted climates, and that biases in specific humidity cannot be simply related to biases in cloud amount and convection. However, these 10-day long simulations were framed with observations, so that their departure from observations was limited. Larger differences with observations are to be expected from more freely conducted simulations.

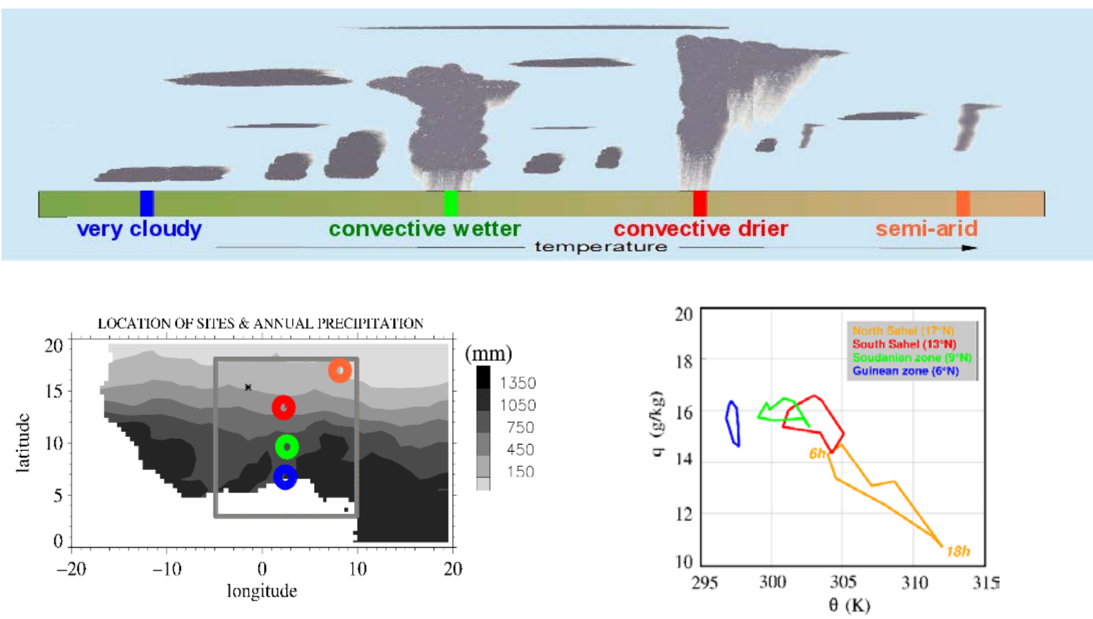

Figure 4.2. *Top: schematic of the change in typical cloud types along the meridional transect during the monsoon, with surface temperature increasing northwards.*
Lower left panel: location of the sites (same color code: blue, green, red, orange, as above); These locations sample the meridional climatic gradient, from the Guinean Coast (blue), the wet tropical Soudanian zone (green), the southern (red) and northern (orange) Sahel during the monsoon.
Lower right panel: Observed joint diurnal fluctuations of potential temperature and water vapour mixing ratio in the lower atmosphere (0-500 m average), 10-day mean values at the four different types of location during the monsoon. Lower panels adapted from Gounou et al. (2012).

With these considerations in mind, the simulation of these regimes in CMIP5 AMIP has been explored, and the differences in surface-boundary layer couplings have been addressed via an analysis of the CFMIP cfSites diagnostics. Not unexpectedly, point to point comparisons of observations and simulations are often complicated by differences in the latitudinal position of the monsoon, and this is of limited interest for our purpose. Only half of the models, namely IPSL-CM5b-lr, HadGEM2-a show a qualitative agreement with observations, in terms of daytime fluctuations (Fig. 4.3). However, Fig. 4.3 also highlights a spread among models in the mean temperature and specific humidity values.

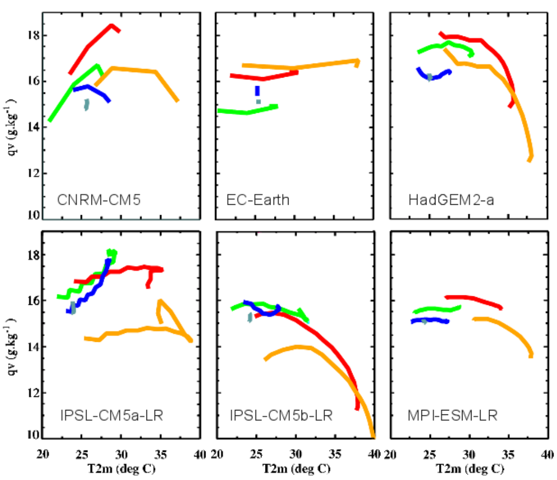

Figure 4.3. *same as Fig. 4.2 lower right panel except for CMIP5 AMIP simulations and august-mean of 30-year series of T2m and q2m. Here, only daytime trajectories, from morning to afternoon are displayed, for clarity.*

Therefore, the simulations have been analyzed using the temperature-water vapour frame of Gounou et al. (2012) and the results have been also further sorted according to additional parameters such as seasonal mean precipitation amount (this a simple way to take into account shifts in the meridional position of the ITCZ). We used the ensemble of cfSites for the study. This methodology appears efficient to get rid of much of the spread in mean values (Fig. 4.4). However, the overall structure of daytime fluctuations is not much changed and the distinct signature of each model is still present (compare results of each model in Figs. 4.3 and 4.4). Note that the problem is really restricted to land areas where the low levels of the atmosphere experience large daytime fluctuations (see the small disk in Fig. 4.4 for the Guinean cfSite).

The monthly-mean diurnal cycle of precipitation and of cumulative surface net radiation is also presented in Fig. 4.4. The amplitude of the diurnal cycle of precipitation and its fluctuations (or lack thereof) is very model-dependent. It is much flatter in CNRM-CM5, EC-Earch than in IPSL-CM5a-lr and IPSL-CM5b-lr. It is noticeable that the diurnal cycle of precipitation shifted later in the day in IPSL-CM5b-lr and IPSL-CM5a-lr, in agreement with Rio et al. (2009, 2013) and Hourdin et al. (2013). The daytime fluctuations of temperature and water vapour in the boundary layer are also in a rather good agreement with observations in this later version of the IPSL climate model. These results are really satisfying as it relies on a physically-based improvement of boundary layer and convective parametrizations.

The morning drop of the specific humidity in HadGEM-2A may be explained by the frequency (coarser that the 30-min model time step) at which the radiative computations are carried out in the model (or at which they are updated when used as input to other parametrizations). We found evidence of such discontinuities in other fields of some models. This type of issue may indeed affect numerous models, but these are difficult to track from 3-hourly model outputs.

Fig. 4.4 also shows that the montly-mean net radiation and precipitation are often positively coupled in the range of selected precipitation amounts (IPSL model and HadGEM-2A). This appears to be in broad agreement with observations, at least for the Sahel (monsoon rainfall less than 600 mm, Guichard et al. 2009 and unpublished material). However, some models display the opposite coupling (in particular CNRM-CM5). This issue is associated with, and possibly explained by, a very northern migration of the ITCZ in this model, and the results may improve with the new version of the model, as the ITCZ is now centred on a more southern latitude (not shown).

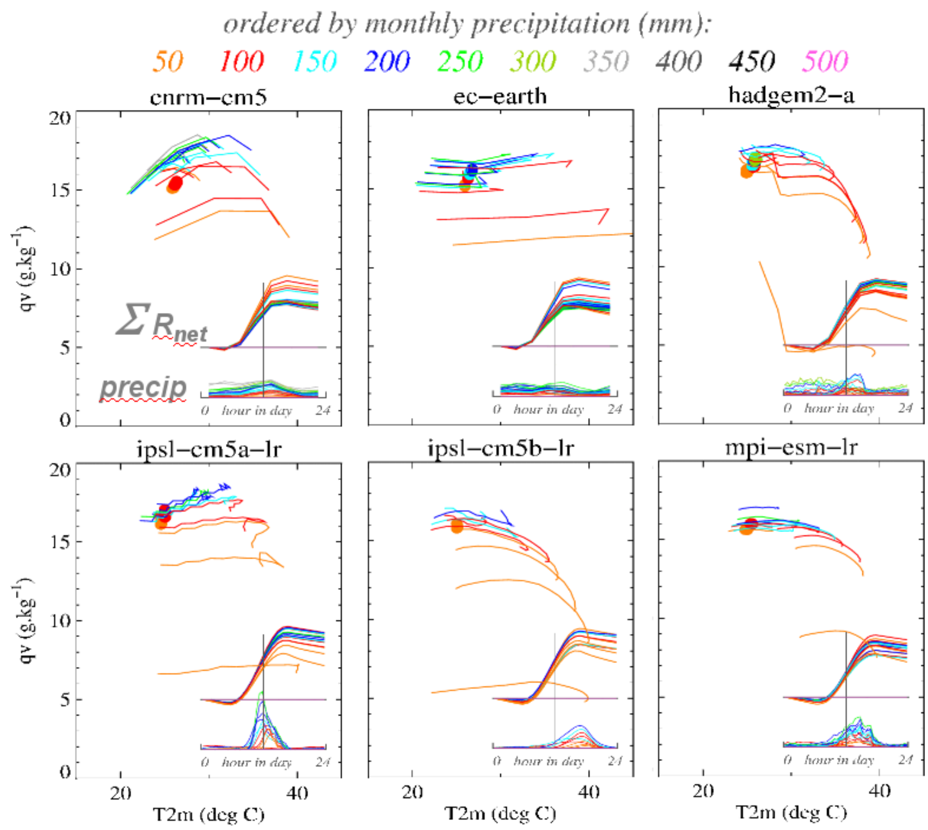

Figure 4.4. *same as Fig. 4.2 lower right panel except for CMIP5 AMIP simulations and august-mean of 30-year series of T2m and q2m. Here, only daytime trajectories, from morning to afternoon are displayed, for clarity. Small disk correspond to the cfSite point in the Gulf of Guinea where diurnal fluctuations are much smaller.*

4.2 An overview of some basic issues with the surface energy budget

The results presented above showed that direct comparison of model results with observations at cfSites are somewhat complicated by differences in the large scale structure of the simulated African Climate. However, some large biases affect the simulation, and these are not explained by such considerations. In particular, the surface energy budget in the Sahelian area display systematic biases illustrated in Fig. 4.5. All models overestimate the surface net radiation (Rnet) in Spring (by several tens of W/m2). Indeed, the spread in net radiation is relatively small compared to the associated very large spread in shortwave incoming radiation (SWin). This may appear surprising, but is explained by compensating balances via the other surface radiative fluxes. Furthermore, this small spread in Rnet is associated with very distinct evaporative fraction and surface sensible and latent heat flux.

This is documented further in Fig. 4.6 for the core of the monsoon season, when Rnet in models is closer to observations (compare the range given by the black symbols to the individual ticks, one color identifies one model). Here, data (black symbols) acquired over few years at two distinct Sahelian sites are used; this allow to almost cover the range of precipitation simulated each year by the different models). However, only in two models (out of six) is the incoming shortwave radiation lying in the range of observations. The different balances between the longwave and shortwave downwelling and upwelling flux is specific to each model. However, in observations, the interannual variations in Rnet and precipitation are closely coupled, while models display a coupling between the interannual variations of precipitation and SWin. As opposed to observations, model display a much larger spread in interannual values of SWin (involving clouds) than in those Rnet. The difference involves the three other components of the surface radiation budget, but notably the upwelling longwave flux (LWup).

Finally, it appears that even the clear-sky SWin estimates vary widely among models (Fig. 4.5, right panel), again by several tens of W/m2. These differences are difficult to explain without consideration of the treatment of aerosols (amount, type and optical properties), and this raises an important issue for the design of future simulations.

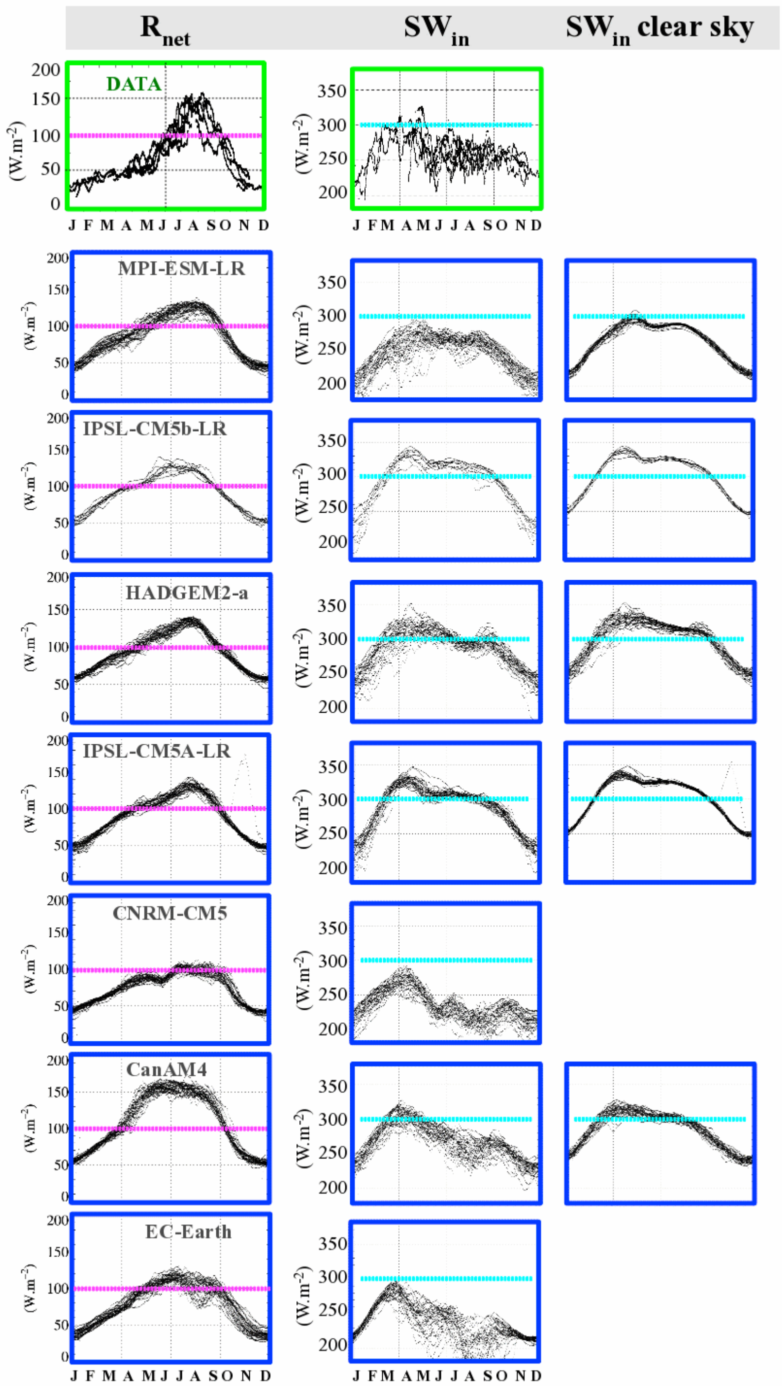

Figure 4.5: Annual cycle of surface net radiation (left column), incoming shortwave flux (middle column) and incoming clear sky shortwave flux (right column) in observations and CMIP5 amip simulations. The different curves correspond to different years (about 30 in simulations). (Here, only the Agoufou cfSite point is shown)

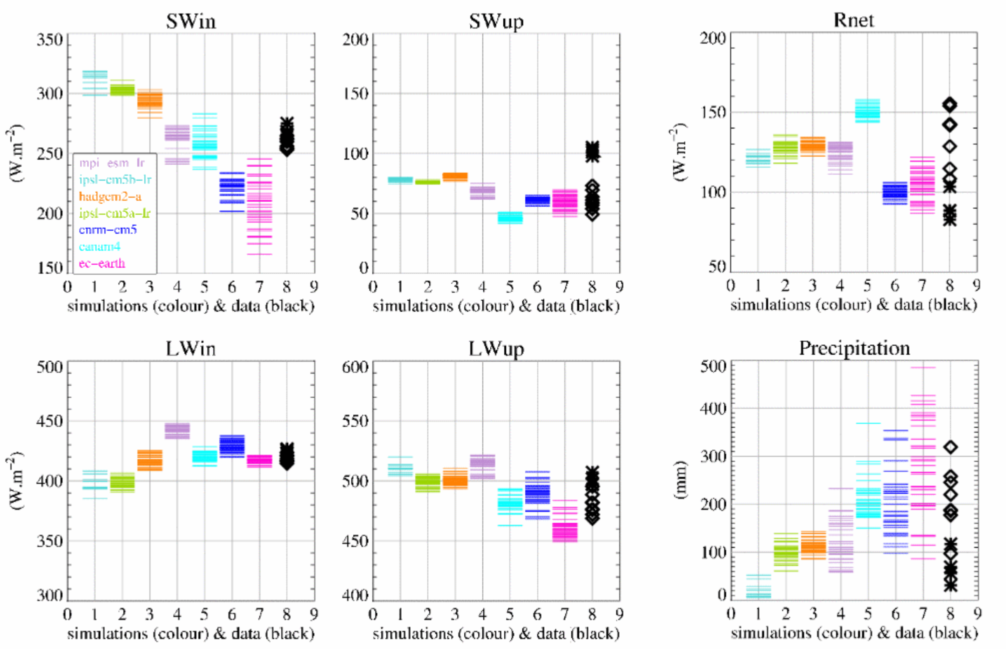

***Figure 4.6** : comparison of the surface radiative fluxes SW_{in} , SW_{up} , LW_{in} , LW_{up} , R_{net} and precipitation. Each color identifies a model, and each horizontal segment corresponds to a different year. The values correspond to a 2-month average, spanning mid-July to mid-September.*

5. Concluding remarks

The results obtained in the study by Neggers and Siebesma (2013) illustrate that the multiple parameter evaluation of continuous, long-term SCM simulations can be an efficient method to (i) constrain a system of interacting parameterizations, (ii) trace impacts of model changes throughout this system, and (iii) reveal the existence of compensating errors between parametric components. In the example documented in this study, this method was applied to evaluate the impact of the implementation of a new boundary layer scheme in the RACMO on the cloud-radiative model climate at Cabauw. The '12-point check' revealed the existence of a compensating error in the interaction of boundary layer clouds and the radiative transfer, residing in the cloud overlap function. The results obtained in this study therefore suggest and emphasize that the important phenomenon of vertical overlap in boundary layer cloud fields is still poorly represented in GCMs, and deserves more scientific research.

In the present-day climate GPCI intercomparison experiment all the SCMs present similar overall biases. The stratocumulus-topped boundary layer in SCMs is too shallow, too moist and too cool. Furthermore the representation of such a regime suffers from an underestimation of the CC and the LWP and an overestimation of the precipitation. These are long-standing issues that have been reported in previous articles on both SCMs and GCMs studies (e.g. Duynkerke et al., 2004; Siebesma et al., 2004). A common representation of the stratocumulus dependence on the free tropospheric conditions is lacking, as the SCMs present a variety of patterns in the phase space defined by LTS and and a similar measure for humidity given by difference between the 700 hPa level and the surface (ΔQ). In particular CC and LWP show large differences from model to model from both a qualitative and quantitative perspective, though none of the SCMs captures the dependence found in the LES results presented in detail by van der Dussen et al. (2014). More precisely none of the models shows a constant CC=1 in the phase space and a main dependence of the LWP on ΔQ with a cloud thinning for drier free tropospheric conditions.

The GPCI intercomparison study highlights that the stratocumulus representation in GCMs is still inadequate. To this end it should be estimated what are the reasons of the inability of GCMs of describing the stratocumulus-topped boundary layer. An accurate analysis of the numerical methods involved in the parametrizations is beyond the interests of the present work but it is for sure an important component. Our analysis is mainly focused on the physical component of the SCMs. The parametrization that contributes the most to the model uncertainties has not been identified. Based on previous studies, we suggest that the lack of the representation of the entrainment at the cloud top as well as the poor representation of microphysical processes might have a key role. Finally independently of the physical parametrizations the vertical resolution seems to be not sufficient to resolve the small variation in the cloud thickness resulting in a LWP decrease found in the LES results. This study is aimed to gained some understanding on the GCMs spread in the future climate predictions. However how representative the results are of the GCM counterpart is still unclear. To this end the dependence of the cloud regime on LTS and ΔQ for several GCMs participating to CMIP5 will be reported in a follow-up paper.

For the West African region, the variations in surface-boundary layer-cloud types and couplings, from the wet Tropics to the Sahara still remains a challenge for models, and the good sampling of the climatic gradient by the cfSites proved to be very useful. These cfSites outputs have been used to design process-based evaluations of climate models, framed by previous observational AMMA studies and more controlled single-column model studies. It appears that the daytime evolution of the surface thermodynamics and its sensitivity to the climate is generally qualitatively reproduced. However, differences among models often dominate over the sensitivity to the climate (framed by mean precipitation and surface net radiation). In fact, the simulation of Rnet is generally much better that the simulation of the incoming shortwave radiation (which involves cloud and aerosol radiative effects) and is associated with very different evaporative fractions in models (linked to rainfall). Additional issues arise from inaccurate surface albedo in some models over the Sahel and Sahara. Overall, the results underline modeling issues which go beyond a problem of simulating deep convection over land. They further point to the need of a more accurate simulation of surface properties and state, aerosols and clouds. This can only be achieved by better physical parametrizations, including the interactions operating between the parametrized processes. The results also underline recent improvements in some current and future models.

References (the papers that are part of D3.6 are depicted in boldface letters).

Bellon, G. and B. Stevens, 2012: Using the sensitivity of large-eddy simulations to evaluate atmospheric-boundary-layer models. *J. Atmos. Sci*., **69**, 1582–1601.

Bouniol, D., F. Couvreux, P.-H. Kamsu-Tamo, M. Leplay, F. Guichard, F. Favot and E. O'Connor, 2012 : Diurnal and seasonal cycles of cloud occurrences, types and radiative impact over West Africa. J. Appl. Met. Clim., 51, 534-553. doi : 10.1175/JAMC-D-11-051.1

Couvreux, F., F. Guichard, A. Gounou, D. Bouniol, P. Peyrillé, and M. Köhler, 2014 : Modelling of the thermodynamical diurnal cycle in the lower atmosphere : a joint evaluation of four contrasted regimes in the Tropics over land. Boundary-Layer Meteorol, 150, 185–214. doi : 10.1007/s10546-013-9862-6.

Dal Gesso, S., A. P. Siebesma, and S. R. de Roode, 2014a: Evaluation of low-cloud climate feedback through single-column model equilibrium states. *Q. J. Royal Meteor. Soc.*, early version published online.

Dal Gesso, S., J. J. van der Dussen, A. P. Siebesma, S. R. de Roode, I. Boutle, H. Kamae, R. Roehrig, J. Vial, 2014b. A Single-Column Model intercomparison on the stratocumulus representation in present-day and future climate.
To be submitted. Available the EUCLIPSE website.

Duynkerke, P.G., et al. 2004: Observations and numerical simulations of the diurnal cycle of the EUROCS stratocumulus case. *Q. J. Royal Meteor. Soc.*, 130, 3269-3296.

Gounou, A., F. Guichard and F. Couvreux, 2012 : Observations of Diurnal Cycles Over a West African Meridional Transect : Pre-Monsoon and Full-Monsoon Seasons. Boundary-Layer Meteorol., 144, 329-357. doi : 10.1007/s10546-012-9723-8

Guichard, F., L. Kergoat, E. Mougin, F. Timouk, F. Baup, P. Hiernaux and F. Lavenu , 2009 : Surface thermodynamics and radiative budget in the Sahelian Gourma : seasonal and diurnal cycles, J. Hydrology, 375, 161-177. doi : 10.1016/j.jhydrol.2008.09.007

Neggers, R. A. J., 2009: A dual mass flux framework for boundary layer convection. Part II: Clouds. *J. Atmos. Sci.*, **66**, 1489–1506.

Neggers, R. A. J., M. Koehler, and A. A. M. Beljaars, 2009: A dual mass flux framework for boundary layer convection. Part I: Transport. *J. Atmos. Sci.*, **66**, 1465–1487.

Neggers, R.A.J., and A. P. Siebesma, 2013: Constraining a system of interacting parameterizations through multiple-parameter evaluation: tracing a compensating error between cloud vertical structure and cloud overlap. *J. Clim*., 26, 6698-6715.

Rieck, M. , L. Nuijens, and B. Stevens, 2012: Marine boundary layer cloud feedbacks in a constant relative humidity atmosphere. *J. Atmos. Sci*., **69**, 2538-2550.

Roehrig, R., D. Bouniol, F. Guichard, F. Hourdin and J.-L. Redelsperger, 2013: The present and future of the West African monsoon: a process-oriented assessment of CMIP5 simulations along the AMMA transect. *J. Climate*, 26, 6471-6505, doi: 10.1175/JCLI-D-12-00505.1

Siebesma, A. P., C. Jakob, G. Lenderink, R. A. J. Neggers, J. Teixeira, E. van Meijgaard, J. Calvo, A. Chlond, H. Grenier, C. Jones, 2004: Cloud representation in general-circulation models over the northern pacific ocean: A EUROCS intercomparison study. *Q. J. Royal Meteor. Soc.*, **130**, 3245-3267.

van der Dussen, J. J. , S. R. de Roode, A. P. Siebesma, and S. Dal Gesso, 2014. Influence of the free troposphere on the response of steady-state stratocumulus cloud amount to a climate perturbation using LES. To be submitted to the *J. Adv. Model. Earth Syst.*

Zhang, M. et al., 2013: CGILS: Results from the first phase of an international project to understand the physical mechanisms of low cloud feedbacks in single column models, *J. Adv. Model. Earth Syst*., **5**, 1-17.